Magnetic-field dependence of low-temperature mobility in quasi-one-dimensional electron systems

Magnetic-field dependence of low-temperature mobility in quasi-one-dimensional electron systems

B Tanatar† and N C Constantinou‡

† Department of Physics, Bilkent University, Bilkent, 06533 Ankara, Turkey
‡ Department of Physics, University of Essex, Colchester CO4 3SQ, UK

Abstract. We study the mobility of a quasi-one-dimensional (Q1D) electron system in the presence of an axial magnetic field at low temperatures. We consider the mobility limits for remote-impurity scattering, homogeneous-background scattering, interface-roughness scattering, and alloy-disorder scattering mechanisms. For a system in which all carriers are in the lowest subband, the electron–impurity interaction is modelled for the above cases, and analytic expressions are derived. Calculations appropriate for a GaAs Q1D structure are presented for typical wire radius R, electron density N, impurity density N_i, and applied magnetic field B.

1. Introduction

New developments in fabrication techniques such as molecular-beam epitaxy (MBE) and lithographic deposition have made possible the realization of quasi-one-dimensional (Q1D) electron systems. In these structures based on the confinement of electrons, the electron gas is quantized in two transverse directions, thus the charge carriers essentially move only in the longitudinal direction. There have been many experimental [1–6] and theoretical [7–11] studies in various aspects of Q1D semiconducting electronic systems in both the absence and presence of the applied magnetic field. Using magnetic depopulation, far-infrared, and Raman spectroscopy techniques, plasmon dispersion in GaAs quantum wires is measured. Extensive experimental [12] and theoretical [13] reviews on Q1D electron systems as realized in semiconductors are available for a detailed discussion.

Hu and Das Sarma [14] have recently shown convincingly the reason one-dimensional (1D) quantum-wire electrons behave as normal Fermi liquids, despite the theoretical claims of the existence of non-Fermi-liquid-type ground states (i.e., Luttinger liquid). Also the experiments by Goñi et al [1] on the intersubband plasmons give strong evidence of Fermi-liquid behaviour. Most of the experiments so far have used the applied field in the transverse direction (i.e., perpendicular to the direction of free motion). In our model the magnetic field B lies along the free direction, thereby making the physics of the problem somewhat different from the transverse-field case. For the analogous Q2D system, in-plane magnetic field effects on the subband structure have been considered theoretically [15, 16] and observed experimentally [17, 18]. Tang and Butcher have investigated the effects of an in-plane magnetic field on the low-temperature parallel [19] and perpendicular [20] transport properties of Q2D systems. There are not too many experiments on Q1D electron systems in which the applied magnetic field is in the longitudinal direction, because of difficulties associated with fabricating uniform wires. In the available measurements [21] novel anisotropies, reflected by the changes in the density of states, are seen. We have recently studied [9] the magnetoplasmon modes in these systems.

Owing to the limited number of available final states during the scattering process, the mobility of Q1D electron systems is considerably enhanced, making them potentially important for high-speed device applications. Since their early prediction by Sakaki [22] and subsequent fabrication [5, 6], there has been a lot of interest in the transport properties of Q1D systems. The hope of achieving very high mobilities by confining even more electrons compared with the Q2D heterojunctions has been the main motivation of the study of Q1D electron systems. The mobility of a semiconducting system at room temperature is often dominated by phonon scattering. On the other hand, at low temperatures ($T \sim 5$ K), there will always be ionized impurities and the mobility will be essentially limited by their presence. Thus it is important to assess the impurity limits to the mobility for various mechanisms for possible device applications.

Sakaki [22] has considered the scattering of charge carriers by ionized impurities located a fixed distance outside the 1D structure, and found that the impurity-limited mobility increases exponentially as the distance between the impurities and the wire is increased. Lee and Spector [23] extended these calculations to include background impurities. Gold and Ghazali [10] obtained analytical results for several models of electron–impurity interaction using approximate wave functions. It is noted that these investigations were carried out for Q1D devices in the absence of a magnetic field. Numerical calculations for the mobility of Q1D systems for impurity scattering were given by Weng and Leburton [24] and Lee and Vassell [25]. Calculations on mobility limits due to electron–phonon interactions in quantum-well wires are also reported [26].

Our aim in this paper is to study the magnetic field dependence of the low-temperature ($T \sim 0$ K) impurity-limited mobility of a Q1D electron system. We use the quantum-well potential model developed recently by Constantinou, Masale, and Tilley [27] to describe the Q1D system in an axial magnetic field. Assuming the size quantum limit (SQL), namely only the lowest subband is occupied by the charge carriers, we calculate the electron–electron and electron–impurity interactions, and provide analytical expressions valid for GaAs in a range of wire-radius R and applied-magnetic-field B values.

The rest of this paper is organized as follows. In section 2 we introduce the wave function, energy levels, and electron–electron and electron–impurity interactions for electrons confined in a cylindrical quantum wire in an external magnetic field B. We also give a simple, approximate expression for the one-electron wave function in the lowest subband. In section 3, using our approximate wave function, we obtain analytical results for the Coulomb and impurity interactions. An analytic expression for the dielectric function $\varepsilon(q)$ when $k_B T \ll E_F$ is used in the calculation of mobility of our quantum-well-wire model. We consider the mobility limits for remote-impurity scattering, homogeneous-background scattering, interface-roughness scattering, and alloy-disorder scattering mechanisms. We conclude in section 4 with a brief summary of our results and comments on further studies.

2. Theory

We consider a model of the electron gas, quantized in two transverse directions, so that the charge carriers can only move in the longitudinal direction. We choose the cross section of the system to be circular with radius R, hence the quantum-wire geometry becomes cylindrical. The external magnetic field is applied parallel to the longitudinal axis. In the SQL, the radius R of the quantum-well wire is much smaller than the thermal de Broglie wavelength of the charge carriers, so that only the ground-state (lowest) subband is populated. In some experiments [2] this limit has been achieved leading towards the goal of

high-mobility devices. Cylindrical wires of radius $R \sim 300$ Å have recently been fabricated by Tonucci *et al* [28]. As will be discussed later, we choose the size parameters in this work such that the SQL is attained and the intersubband scattering that otherwise would be important [22] is completely neglected. The key parameter in the description of the motion of an electron in a magnetic field is the ratio l_B/R, where $l_B^2 = \hbar c/eB$ is the cyclotron radius. For $l_B \ll R$, the electron is strongly confined by the magnetic field, whereas in the opposite limit $l_B \gg R$ the confinement due to B becomes unimportant [27]. In the model of an infinite potential well confining the charge carriers, the effective-mass wave function is given by [27, 29]

$$\psi \sim \exp\left(-\xi/2\right)\xi^{|m|/2}M(a, b, \xi)e^{im\theta} \qquad (1)$$

where $\xi = r^2/2l_B^2$ is a dimensionless variable, and $M(a, b, \xi)$ is the confluent hypergeometric function with the arguments defined as $a = -E_{ml}/\hbar\omega_c + \frac{1}{2}(1 + m + |m|)$, and $b = |m| + 1$. The eigenvalues E_{ml} are obtained by solving $M(a, b, R^2/2l_B^2) = 0$, with the index l denoting the lth root. Other models with the same geometry such as parabolic confinement of electrons yield qualitatively similar results.

We introduce the following approximate form to the wave functions appropriate for the lowest states (viz., $l = 1$, and $m = 0, \pm1, \ldots$):

$$\psi \sim (1 - r^2/4l_B^2)(r^2/2l_B^2)^{|m|/2}(1 - r^2/R^2)e^{im\theta} \qquad (2)$$

which satisfy the condition $\psi(R) = 0$. The normalization constants here are different from those for the full wave functions, and may be evaluated analytically. We have found that these approximate wave functions are in good agreement with the exact ones for a range of B and R values for practical purposes. They allow us to calculate the Coulomb and impurity interaction matrix elements analytically.

The Coulomb interaction and impurity scattering matrix elements between the subbands are given respectively by

$$V_{ijkl}(q) = \frac{2e^2}{\kappa} \int d^2r \int d^2r' \, \psi_i^*(r)\psi_j(r)K_0(q|r - r'|)\psi_k^*(r')\psi_l(r') \qquad (3)$$

and

$$V_{ij}(q) = -\frac{2e^2}{\kappa} \int d^2r \, \psi_i^*(r)\psi_j(r)K_0(q|R_i - r|) \qquad (4)$$

where $K_0(x)$ is the modified Bessel function of the second kind, and κ is the background dielectric constant. In the electron–impurity interaction we assume that an impurity is located at R_i.

We express the relaxation time τ_t in terms of the electron–impurity potential and the static dielectric function $\varepsilon(q)$ as [26]

$$\frac{1}{\tau_t} = \frac{k_F}{\hbar E_F} \frac{\langle |U(2k_F)|^2 \rangle}{\varepsilon(2k_F)^2}. \qquad (5)$$

The *average* of the impurity scattering matrix elements above will be defined for various mechanisms later. The Fermi wave vector k_F and the Fermi energy E_F are taken to be those given by the zero-field values ($k_F = \pi N/2$, where N is the number of electrons per unit length) since their dependence on field strength is weak [30]. The relaxation time determines the mobility at zero temperature by the following expression:

$$\mu = e\tau_t/m^*. \qquad (6)$$

In this study, we do not evaluate the relaxation time τ_t directly, but use models for the impurity potential $\langle U^2 \rangle$ to calculate μ. Recently, Masale and Constantinou [31] have calculated the magnetic-field-dependent scattering time τ_s due to electron–phonon interactions in Q1D systems.
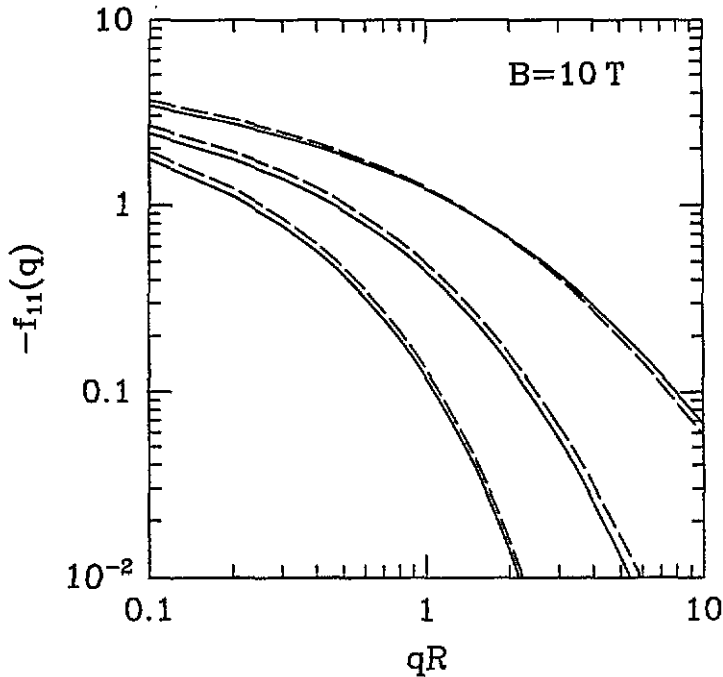
Figure 1. The electron–impurity interaction at $B = 10$ T for $R_i = 0$ (upper curves), $R_i = R$ (middle curves), and $R_i = 2R$ (lower curves). Solid and dashed lines correspond to the exact and analytical results, respectively.

3. Results and discussion

In order to discuss our numerical results on the impurity-limited mobility, we employ material parameters appropriate for GaAs, with electron effective mass $m^* = 0.067\, m_e$, dielectric constant $\kappa = 12.9$, and a temperature of 5 K. Using the approximate wave functions introduced in the previous section we calculate the Coulomb and impurity-scattering matrix elements analytically in the lowest subband as

$$
\begin{aligned}
f_{1111}(q) = {} & \frac{1}{(1 - \xi_R/4)^2} \frac{36}{(qR)^2} \left[\left[\frac{1}{10} - \frac{2}{3(qR)^2} + \frac{32}{3(qR)^4} - \frac{64}{(qR)^4} I_3(qR) K_3(qR) \right] \right. \\
& - \xi_R \left[\frac{1}{30} - \frac{2}{15(qR)^2} + \frac{16}{3(qR)^4} - \frac{128}{(qR)^4} K_3(qR) \left[I_3(qR) - \frac{6}{qR} I_4(qR) \right] \right] \\
& + \xi_R^2 \left[\frac{1}{210} - \frac{1}{15(qR)^2} + \frac{64}{15(qR)^4} + \frac{96}{(qR)^6} - \frac{64}{(qR)^4} \right. \\
& \left. \left. \times \left[I_3(qR) - \frac{6}{qR} I_4(qR) \right] \left[K_3(qR) + \frac{6}{qR} K_4(qR) \right] \right] \right]
\end{aligned}
\tag{7}
$$

and

$$
f_{11}(q) = -\frac{48}{(1 - \xi_R/4)} \frac{K_0(qR_i)}{(qR)^3} \left[(1 + \xi_R) I_3(qR) - \frac{6\xi_R}{qR} I_4(qR) \right]
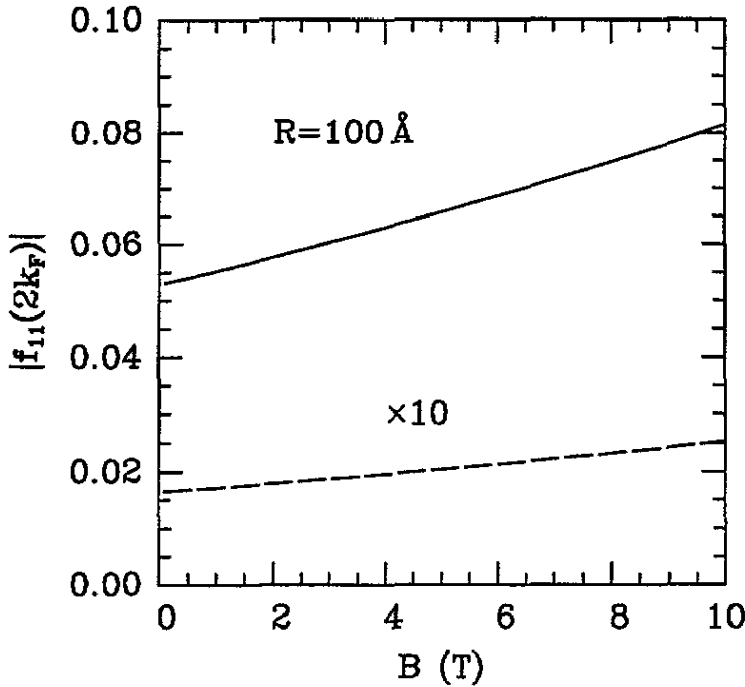\tag{8}
$$

Figure 2. The electron–impurity interaction as a function of B for $R_i = R$ (solid curve), $R_i = 2R$ (dashed curve).

where we have used the definitions $V_{1111}(q) = (2e^2/\kappa)f_{1111}(q)$ and $V_{11} = (2e^2/\kappa)f_{11}(q)$. In the above equations $\xi_R = R^2/2l_B^2$ and the expression for $f_{11}(q)$ is valid when $R_i \geqslant R$. Since $\xi_R \sim B$, the magnetic-field-dependent matrix elements discussed above reduce to the Gold and Ghazali [10] zero-field results as $B \to 0$. Similarly, we obtain an analytical expression for the electron–impurity matrix element when the impurity is within the wire, viz., $R_i < R$,

$$f_{11}(q) = -\frac{48}{(1-\xi_R/4)}\frac{1}{(qR)^2}\left[\frac{1}{8} - \frac{1}{4}\frac{R_i^2}{R^2} + \frac{1}{8}\left[\frac{R_i^2}{R^2} + \frac{8}{(qR)^2}\right]^2 - \frac{1}{(qR)^2} - \frac{I_0(qR_i)K_3(qR)}{qR}\right.$$

$$+ \xi_R\left[\frac{1}{8}\left[\frac{R_i}{R} - \frac{R_i^3}{R^3}\right]^2 + \frac{1}{2(qR)^2}\left[1 - 8\frac{R_i^2}{R^2} + 9\frac{R_i^4}{R^4}\right] - \frac{16}{(qR)^4}\left[1 - \frac{9}{2}\frac{R_i^2}{R^2}\right]\right.$$

$$\left.\left. + \frac{288}{(qR)^6} - \frac{I_0(qR_i)}{qR}\left[K_3(qR) + \frac{6}{qR}K_4(qR)\right]\right]\right]. \tag{9}$$

Again, the analogous result of Gold and Ghazali [10] is obtained as $B \to 0$. We illustrate the adequacy of our approximate wave functions and the resulting analytical expressions for the electron–impurity potential, in figure 1. In this figure, we show the electron–impurity interaction for the impurity distance $R_i = 0$ (upper curves), $R_i = R$ (middle curves), and $R_i = 2R$ (lower curves). Solid and dashed lines indicate exact and analytical results, respectively, and as seen, we obtain close agreement. Similarly, a close agreement is obtained between the exact (equation (3)) and approximate (equation (7)) calculations of $f_{1111}(q)$. It is of interest for the low-temperature mobility to evaluate $f_{11}(2k_F)$ as a function
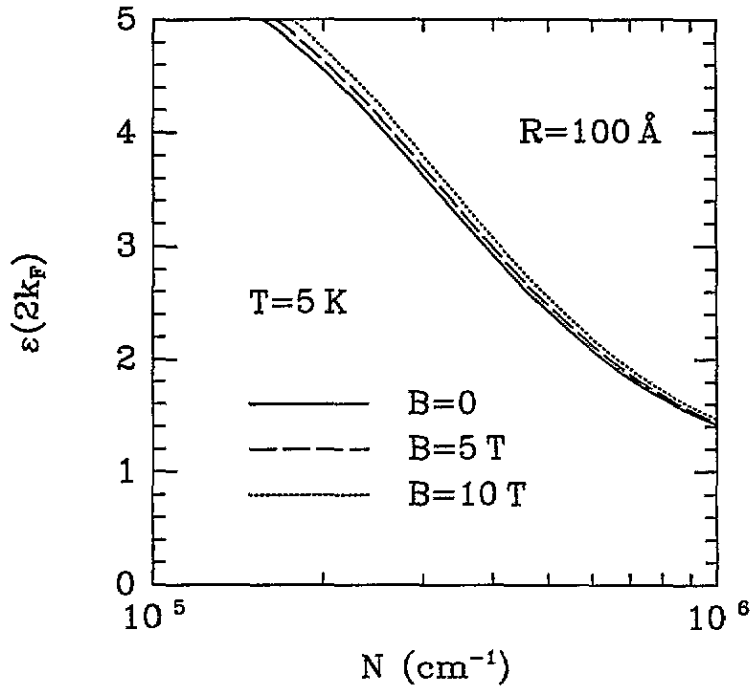
Figure 3. The RPA dielectric function $\varepsilon(2k_F)$ as a function of electron density N for an $R = 100$ Å wire.

of magnetic field B and this is depicted in figure 2 using equations (8) and (9). As is seen the magnetic field tends to increase the electron–impurity interaction, although, for the magnetic fields shown, the effect is not too great.

It is well known that the dielectric function $\varepsilon(q)$ for a 1D system diverges at $q = 2k_F$ signaling the Peierls instability. To circumvent this we use the dielectric function of a Q1D electron system at finite temperatures [32, 33] within the RPA which is given by

$$\varepsilon(2k_F) = 1 + \left(\frac{2}{\pi\kappa}\right)\frac{f_{1111}(2k_F)}{a_B k_F}S(E_F/k_B T) \tag{10}$$

where $a_B = \hbar^2/m^* e^2$ is the Bohr radius defined in terms of the effective mass, and

$$S(x) = \frac{1}{2}\int_0^\infty dt \ln\left|\frac{\sqrt{t} + \sqrt{x/2}}{\sqrt{t} - \sqrt{x/2}}\right|[\cosh^2(t - x/2)]^{-1}. \tag{11}$$

For $E_F \gg k_B T$ (k_B is the Boltzmann constant), the function $S(x)$ may be approximated by [32,33]

$$S(x) = \ln\left(\frac{8e^\gamma x}{\pi}\right) \tag{12}$$

where $\gamma = 0.577\ldots$ is the Euler–Mascheroni constant, and with the help of equation (12) we arrive at an analytic expression for $\varepsilon(2k_F)$. In figure 3 we illustrate the dependence of the dielectric function on carrier concentration. We note that, although its dependence on carrier concentration is significant, its dependence on B is rather weak (at least for fields up to 10 T).
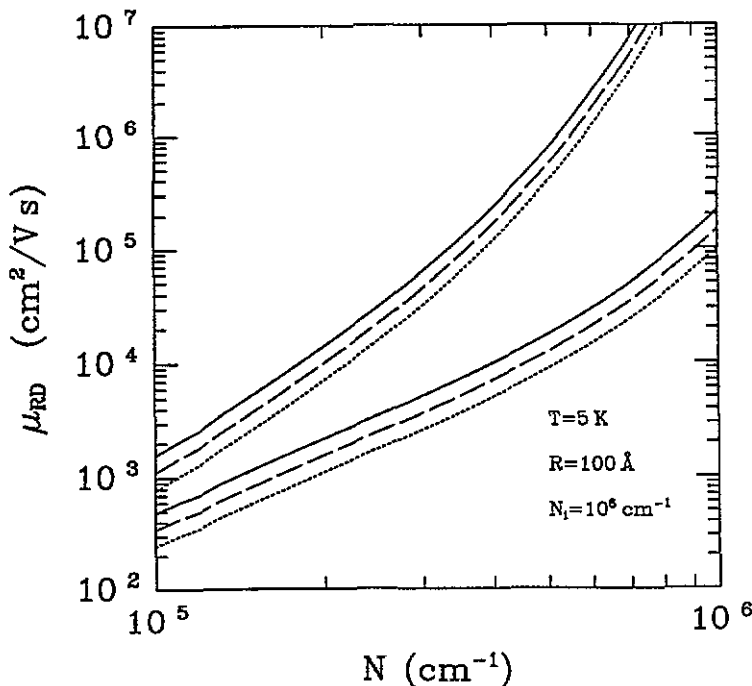
Figure 4. Mobility μ_{RD} due to remote doping as a function of the ID electron density N. We consider an uncompensated semiconductor with $N = N_i = 10^6$ cm^{-1}. Solid, dashed, and dotted lines indicate $B = 0$, 5, and 10 T, respectively, for a 100 Å wire. The upper and lower curves correspond to $R_i = 2R$ and $R_i = R$, respectively.

3.1. Remote doping

For remote impurities located outside the wire, we model the random impurity potential by [10] $\langle U^2 \rangle = N_i[V_{11}(q)]^2$, where N_i is the (one-dimensional) impurity density. The mobility for remote doping is expressed as

$$\mu_{RD} = \left(\frac{e}{\hbar}\right) a_B^2 \left(\frac{\pi \kappa^2}{16}\right) \frac{N}{N_i} \left[\frac{\varepsilon(2k_F)}{f_{11}(2k_F)}\right]^2 \tag{13}$$

In figure 4 we show the calculated μ_{RD} as a function of the 1D electron density N for the magnetic field values $B = 0$ (solid), 5 (dashed), and 10 T (dotted). The upper and lower curves are for $R_i = 2R$ and $R_i = R$, respectively. We took the wire radius $R = 100$ Å, and the impurity density $N_i = 10^6$ cm^{-1}. As expected from physical reasons the further the impurities are from the electron gas, the higher is mobility. Also the magnetic field tends to reduce the mobility somewhat. Mobility for remote doping as a function of the magnetic field is displayed in figure 5. Typically, the mobility drops by a factor of two from its zero field value to its value at 10 T.

3.2. Interface-roughness scattering

It is known that for 2D-semiconductor-based electron systems the interface-roughness scattering is the dominant scattering mechanism. The importance of this mechanism has been illustrated by Sakaki *et al* [34] for 2D systems, and by Motoshisa and Sakaki [35]
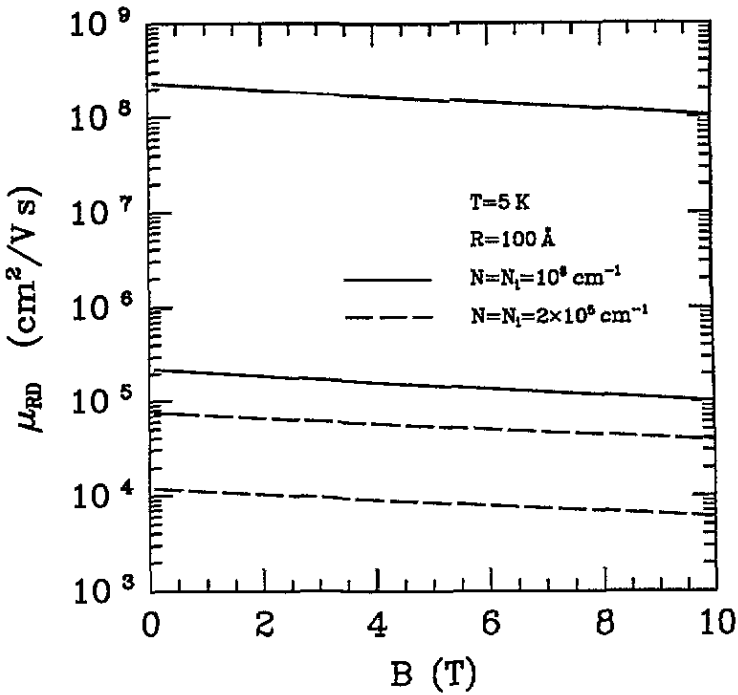
Figure 5. Mobility μ_{RD} due to remote doping as a function of magnetic field B. The higher mobility curves are for $R_i = 2R$ with the lower mobility corresponding to $R_i = R$.

for QID systems. To calculate the mobility for interface-roughness scattering we use the following expression of the random potential [10]

$$\langle U^2 \rangle = \left(\frac{dE_{01}}{dR} \right)^2 \eta \delta^2 \sqrt{\pi} e^{-q^2 \eta^2 / 4}. \tag{14}$$

Here δ and η are the height and range parameters of the roughness, respectively. δ describes the roughness fluctuation amplitude, and η the correlation length. In keeping with the rest of the calculations in this article we only consider the interface-roughness scattering in the first subband, although extension to higher subbands is also possible. The magnetic-field-dependent energy levels may be approximated by the formula given by Dingle [36]

$$E_{ml} = \frac{\hbar^2}{2m^* R^2} t_{ml}^2 + \frac{1}{2} m \hbar \omega_c + \frac{1}{24} \hbar \omega_c (R/l_B)^2 \left[1 + \frac{2(m^2 - 1)}{t_{ml}^2} \right] \tag{15}$$

in which t_{ml} is the lth root of the Bessel function $J_m(x)$, and $\omega_c = eB/m^*$ is the cyclotron frequency. Using the above expression we obtain for the interface-roughness scattering mobility

$$\mu_{IR} = \left(\frac{e}{\hbar} \right) E_R^2 \frac{NR^6}{4\eta\delta^2} \sqrt{\pi} e^{k_F^2 \eta^2} \frac{[\varepsilon(2k_F)]^2}{(E_{01} - 2E_R t_{01}^2)^2} \tag{16}$$

with $E_R = \hbar^2/(2m^* R^2)$. Figure 6 shows the mobility for interface-roughness scattering as a function of the carrier density N. Again the mobility decreases by a factor of two as in the previous case.
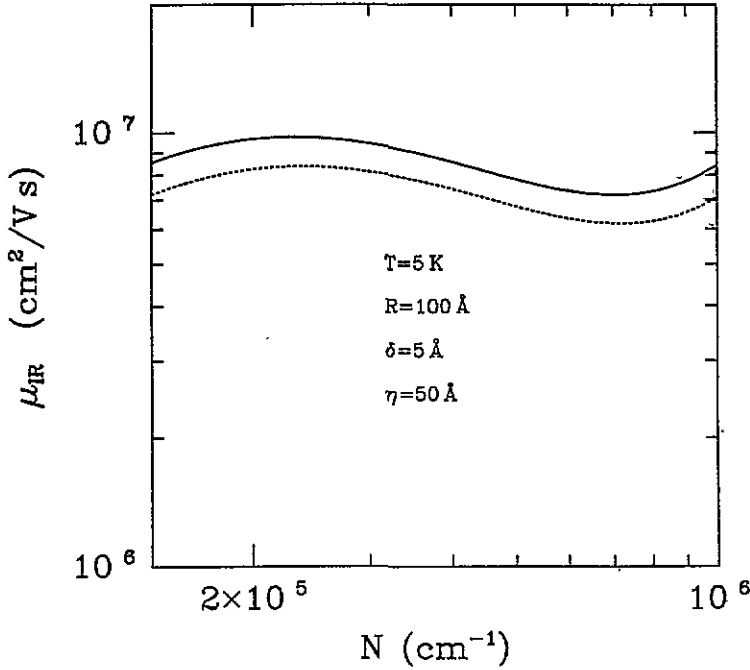
Figure 6. Mobility μ_{IR} due to interface roughness as a function of the carrier density N for $B = 0$ (solid) and 10 (dotted) T.

3.3. Background doping

We now study the mobility due to homogeneous-background doping considering two models. In the first model, impurities are homogeneously distributed inside the wire ($0 < R_i < R$), with a 3D impurity density $N_B^{(1)}$. For our second model we assume that the impurities are homogeneously distributed outside the wire ($R_i > R$), with a 3D impurity density $N_B^{(2)}$. The random potential is defined as

$$\langle U^2 \rangle^{(1,2)} = N_B^{(1,2)} \left(\frac{2e^2}{\kappa} \right)^2 \int_{0,R}^{R,\infty} dR_i \, R_i [f_{11}(q)]^2. \tag{17}$$

The mobility for homogeneous-background doping for both models becomes

$$\mu_{BD}^{(1,2)} = \left(\frac{e}{\hbar} \right) a_B^2 \left(\frac{\pi\kappa^2}{16} \right) \frac{N}{N_B^{(1,2)} R^2} \frac{[\varepsilon(2k_F)]^2}{g_{11}^{(1,2)}(2k_F)} \tag{18}$$

where we have defined

$$g_{11}^{(1,2)}(q) = \int_{0,1}^{1,\infty} dx \, x [f_{11}(q)]^2. \tag{19}$$

Using the approximate wave functions introduced in section 2 we evaluate the above integrals. When the impurities are homogeneously distributed within the wire (model 1) we
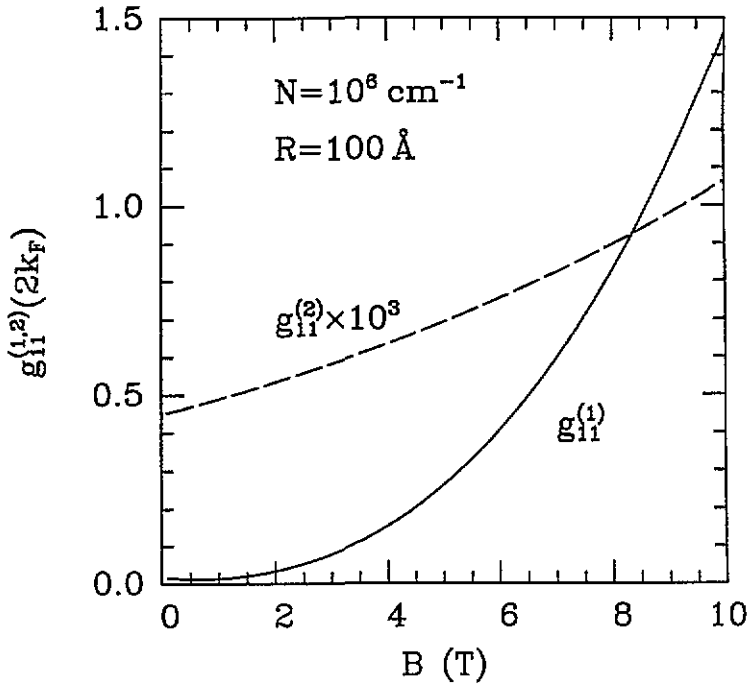
Figure 7. The electron–impurity potentials used in models 1 and 2 for background doping, $g_{11}^{(1,2)}(2k_F)$, as a function of magnetic field B.

obtain

$$
g_{11}^{(1)}(q) = \frac{(48)^2}{2(1-\xi_R/4)^2} \frac{1}{(qR)^6} \left[\frac{(qR)^2}{320} - \frac{1}{24} + \frac{1}{(qR)^2} + \frac{64}{(qR)^6} \right.
$$

$$
+ \xi_R \left[\frac{(qR)^2}{192} + \frac{1}{12} + \frac{1}{6(qR)^4} + \frac{320}{(qR)^6} + \frac{2^9 3^2}{(qR)^8} \right]
$$

$$
+ \xi_R^2 \left[\frac{117(qR)^2}{35 \times 2^6} - \frac{71}{40} + \frac{421}{15(qR)^2} - \frac{120}{(qR)^4} + \frac{896}{(qR)^6} + \frac{2^8 3^2 5}{(qR)^8} + \frac{2^{10} 3^4}{(qR)^{10}} \right]
$$

$$
+ \left[(1+\xi_R)K_3(qR) + \frac{6\xi_R}{qR} K_4(qR) \right]^2 [[I_0(qR)]^2 - [I_1(qR)]^2]
$$

$$
+ \left[(1+\xi_R)K_3(qR) + \frac{6\xi_R}{qR} K_4(qR) \right]\left[\frac{I_0(qR)}{(qR)^3} \left[32 + 8\xi_R \left[(qR)^2 + \frac{72}{(qR)^2} \right] \right] \right.
$$

$$
\left. \left. - \frac{8I_1(qR)}{(qR)^2} \left[1 + \frac{12}{(qR)^2} + \xi_R \left[\frac{(qR)^2}{4} + \frac{1}{2} + \frac{37}{(qR)^2} + \frac{288}{(qR)^4} \right] \right] \right] \right] \tag{20}
$$

and for impurities homogeneously distributed outside the wire (model 2)

$$
g_{11}^{(2)}(q) = \frac{(48)^2}{2(1-\xi_R/4)^2} \frac{[(1+\xi_R)I_3(qR) - 6\xi_R I_4(qR)/(qR)]^2}{(qR)^6} [[K_1(qR)]^2 - [K_0(qR)]^2].
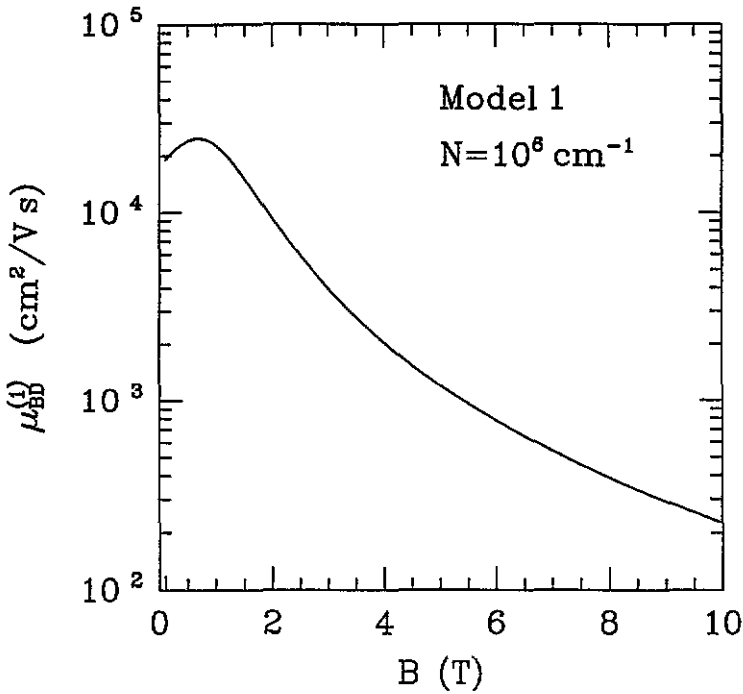$$

$$
\tag{21}
$$

Figure 8. Mobility μ_{BD} due to background doping of model 1, as a function of B, for $R = 100$ Å.

We plot in figure 7 the magnetic-field dependence of $g_{11}^{(1,2)}(2k_F)$. It is predicted that $g_{11}^{(2)}$ varies by a factor of two over the range of B considered but the variation of $g_{11}^{(1)}$ is even more pronounced. These differences, as we shall see, manifest themselves in the mobility. The results of our calculation of $\mu_{BD}^{(1)}$ are displayed in figure 8 as a function of magnetic field B, where we used $N_B^{(1)} = 2 \times 10^6/R^2$ cm^{-3} for the 3D impurity density. We predict a drop in the mobility by two orders of magnitude due to the the behaviour of $g_{11}^{(1)}$ with B. In figure 9 we show the mobility for homogeneous-background doping of our model 2. We have used $N_B^{(2)} R^2/2 = N$ for charge neutrality in uncompensated semiconductors, and the upper and lower curves in figure 9 correspond to $R = 100$ and 50 Å. As in model 1 the mobilities decrease, but in this case it is only by an order of magnitude due to the weaker variation in $g_{11}^{(2)}$.

3.4. Alloy-disorder scattering

Following the model for alloy-disorder scattering developed by Ando [37] for 2D systems, and that extended by Gold and Ghazali [38] to QID systems, we express the random potential as $\langle U^2 \rangle = (\delta V)^2 x(1-x) F_{AD}/4a_B^2$. Here δV is the root-mean-square spatial average of the fluctuating alloy potential, and F_{AD} is the form factor defined by

$$F_{AD} = a_B^2 \int d^2r \, |\psi(r)|^4 \tag{22}$$

where $\psi(r)$ is the wave function for the electrons in the lowest subband. Using our approximate form to the wave function, we obtain
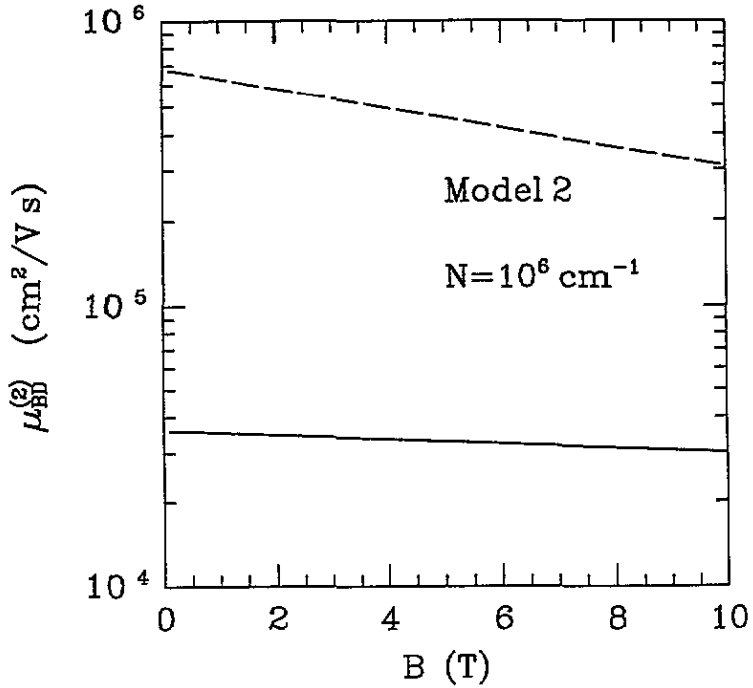
Figure 9. Mobility μ_{BD} due to background doping of model 2, as a function of B for $R = 50$ Å (solid), and $R = 100$ Å (dashed).

$$F_{AD} = \left(\frac{a_B}{R}\right)^2 \frac{3}{35\pi} \frac{(21 - 7\xi_R + \xi_R^2)}{(1 - \xi_R/4)^2} \tag{23}$$

which reduces to the Gold and Ghazali [38] result in the $B = 0$ limit. The mobility for alloy-disorder scattering becomes

$$\mu_{AD} = \left(\frac{e}{\hbar}\right) a_B^2 4\pi N a_B \frac{[\varepsilon(2k_F)]^2}{(\delta V)^2 x(1 - x) F_{AD}} \tag{24}$$

in which the fluctuating alloy potential δV is in units of effective Rydbergs (Ryd=$e^2/2a_B$). In figure 10 we show the wire-radius dependence of alloy-disorder scattering-limited mobility for an $Al_x Ga_{1-x}As$ semiconductor wire. We took the Al concentration to be $x = 0.3$, and fluctuating alloy potential $\delta V = 1$ meV. Solid, dashed, and dotted curves are for $B = 0$, 5, and 10 T, respectively. We observe that the magnetic field dependence of μ_{AD} is not very strong, although interestingly, the magnetic field leads to an increase in the mobility (although very weak), in contrast to the other cases. Our calculations were performed for carrier density of $N = 10^6$ cm^{-1}, and only the lowest subband is assumed to be filled. When $N \geqslant 2/R$, the population of higher subbands should also be taken into account [10].

4. Summary

In this paper we have investigated the magnetic-field dependence of the impurity-limited mobility in QID electron systems. For a model of the QID system we considered a quantum-well wire in a cylindrical geometry and assumed that an external field is applied in the axial
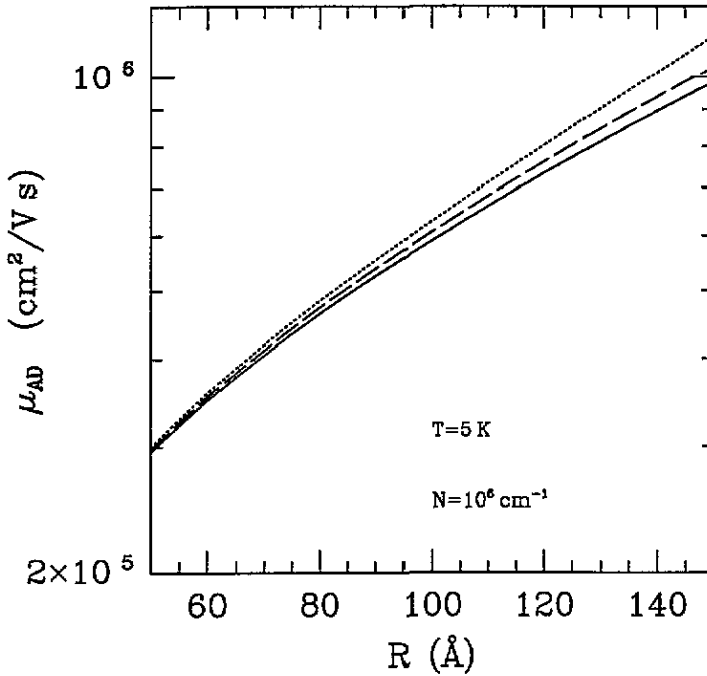
Figure 10. Mobility μ_{AD} due to alloy-disorder scattering, as a function of the wire radius R at $N = 10^6$ cm^{-1} for $B = 0$ (solid), 5 (dashed), and 10 (dotted) T.

direction. Introducing approximate wave functions we obtained analytical expressions for the magnetic-field-dependent electron–impurity interaction and impurity-limited mobility, which might be useful to the experimentalists. It is noted here that these analytic expressions for the mobility derived in the previous sections agree with the exact numerical results to a very good degree. Electron–impurity interactions are used to construct models for remote doping, interface-roughness scattering, homogeneous-background doping, and alloy-disorder scattering. We find that the various mobilities are lowered with increasing magnetic field (except for alloy disorder), with typically a factor of two reduction at 10 T.

Our calculations were performed within the random phase approximation and assuming only the first subband is occupied (the so-called extreme quantum limit). This latter assumption needs some justification. Theoretical results by Nixon and Davies [39] predict that in a split-gate structure the one-dimensional electron gas is strongly distorted by the random potential of the impurities and undergoes a metal–insulator transition before reaching the extreme quantum limit. Nikolic and MacKinnon have also recently considered localization effects in some detail for a different type of quantum wire [40]. On the other hand, the experiments by Goni *et al* [1] clearly demonstrate the realization of the extreme quantum limit and further observe the plasmon modes which are a clear indication of Fermi-liquid behaviour.

In the calculations for zero-field mobility Gold and Ghazali [10] found that local-field corrections to the electron–electron interactions at $N \sim 10^5$ cm^{-1} tend to reduce the mobility. This approach goes beyond the RPA. We have not investigated the local-field effects on the mobility in the presence of a magnetic field, but such effects could be incorporated in our calculations. It would also be interesting to study the temperature dependence of the impurity-limited mobility. There are not many experiments on QID

semiconducting electron systems in the presence of an axial magnetic field. We hope our theoretical considerations will motivate such experiments in the future.

Acknowledgments

References

[1] Göni A R, Pinczuk A, Weiner J S, Calleja J M, Dennis B S, Pfeiffer L N and West K W 1991 *Phys. Rev. Lett.* **67** 3298
     Demel T, Heitmann D, Grambow P and Ploog K 1988 *Phys. Rev. B* **38** 12732
     Egeler T, Abstreiter G, Weimann G, Demel T, Heitmann D, Grambow P and Schlapp W 1990 *Phys. Rev. Lett.* **65** 1804
[2] Plaut A S, Lage H, Grambow P, Heitmann D, von Klitzing K and Ploog K 1991 *Phys. Rev. Lett.* **67** 1642
[3] Berggren K F, Thornton T J, Newson D J and Pepper M 1986 *Phys. Rev. Lett.* **57** 1769
[4] Hansen W, Horst H, Kotthaus J P, Merkt U, Sikorski C and Ploog K 1987 *Phys. Rev. Lett.* **58** 2586
     Demel T, Heitmann D, Grambow P and Ploog K 1991 *Phys. Rev. Lett.* **66** 2657
     Alsmeier J, Sikorski C and Merkt U 1988 *Phys. Rev. B* **37** 6547
[5] Thornton T J, Pepper M, Ahmed H, Andrews D and Davies G J 1986 *Phys. Rev. Lett.* **56** 1198
     Cibert J, Petroff P M, Dolan G J, Pearton S J, Gossard A C and English J H 1986 *Appl. Phys. Lett.* **49** 1275
     Temkin H, Dolan G J, Parish M B and Chu S N G 1987 *Appl. Phys. Lett.* **40** 413
     Iafrate G J, Kerry D K and Reich R K 1982 *Surf. Sci.* **113** 485
[6] Petroff P H, Gossard A C, Logan R A and Wiegmann W 1982 *Appl. Phys. Lett.* **45** 635
[7] Li Q and Das Sarma S 1989 *Phys. Rev. B* **40** 5860; 1991 *Phys. Rev. B* **43** 11768; 1991 *Phys. Rev. B* **44** 6277
[8] Li Q and Das Sarma S 1990 *Phys. Rev. B* **41** 10268
     Gold A 1992 *Z. Phys.* **89** 213
[9] Tanatar B and Constantinou N C 1993 *Phys. Rev. B* **48** 18280
[10] Gold A and Ghazali A 1990 *Phys. Rev. B* **41** 7626
[11] Leburton J P 1984 *J. Appl. Phys.* **56** 2850
[12] Hansen W 1991 *Quantum Coherence in Mesoscopic Systems (NATO ASI Series 254)* ed B Kramer (New York) p 23
[13] Bastard G, Brum J A and Ferreira R 1991 *Solid State Phys.* **44** 229
[14] Hu B Y-K and Das Sarma S 1992 *Phys. Rev. Lett.* **68** 1750; 1993 *Phys. Rev. B* **48** 5469
[15] Maan J C 1984 *Two-dimensional Systems, Heterostructures, and Superlattices* ed G Bauer *et al* (Berlin: Springer)
[16] Merlin R 1984 *Solid State Commun.* **64** 99
[17] Maan J C, Uihlein Ch, Chang L L and Esaki L 1982 *Solid State Commun.* **44** 653
[18] Brummell M A, Hopkins M A, Nicholas R J, Portal J C, Cheng K Y and Cho A Y 1986 *J. Phys. C: Solid State Phys.* **19** L107
[19] Tang H and Butcher P N 1988 *J. Phys. C: Solid State Phys.* **21** 3313
[20] Tang H and Butcher P N 1988 *J. Phys. C: Solid State Phys.* **21** 3959
[21] Smith T P III, Brum J A, Hong J M, Knoedler C M, Arnot H and Esaki L 1988 *Phys. Rev. Lett.* **61** 585
     Hansen W, Smith III T P, Lee K Y, Brum J A, Knoedler C M, Hong J M and Kern D P 1989 *Phys. Rev. Lett.* **62** 2168
[22] Sakaki H 1980 *Japan. J. Appl. Phys.* **19** L735; 1981 *J. Vac. Sci. Technol.* **19** 148
[23] Lee J and Spector H N 1983 *J. Appl. Phys.* **54** 3921
[24] Weng Y and Leburton J P 1989 *J. Appl. Phys.* **65** 3089
[25] Lee J and Vassell M O 1984 *J. Phys. C: Solid State Phys.* **17** 2525

[26] Fishman G 1986 *Phys. Rev.* B **34** 2394
      Hu G Y and O'Connell R F 1991 *J. Phys.: Condens. Matter* **3** 4633
[27] Constantinou N C, Masale M and Tilley D R 1992 *J. Phys.: Condens. Matter* **4** 4499
      Masale M, Constantinou N C and Tilley D R 1992 *Phys. Rev.* B **46** 15432
[28] Tonucci R J, Justus B L, Campillo A J and Ford C E 1992 *Science* **258** 783
[29] Branis S V, Li G and Bajaj K K 1993 *Phys. Rev.* B **47** 1316
      Rensink M E 1969 *Am. J. Phys.* **37** 900
[30] Kelly M J 1989 *J. Phys.: Condens. Matter* **1** 7635
[31] Masale M and Constantinou N C 1993 *Phys. Rev.* B **48** 11 128
[32] Maldague P 1978 *Surf. Sci.* **73** 296
[33] Lee J and Spector H N 1985 *J. Appl. Phys.* **57** 366
[34] Sakaki H *et al* 1987 *Appl. Phys. Lett.* **51** 1934
[35] Motoshisa J and Sakaki H 1992 *Appl. Phys. Lett.* **60** 1315
[36] Dingle R B 1952 *Proc. R. Soc.* A **212** 47
[37] Ando T 1982 *J. Phys. Soc. Japan* **51** 3900
[38] Gold A and Ghazali A 1992 *Solid State Commun.* **83** 661
[39] Nixon J A and Davies J H 1990 *Phys. Rev.* B **41** 7929
[40] Nikolic K and MacKinnon A 1993 *Phys. Rev.* B **47** 6555